FIBREOPTIC COMMUNICATION

PACS numbers: 42.79.Sz; 42.81.Dp
DOI: 10.1070/QE2007v037n06ABEH013448

Study of high-bit-rate fibreoptic communication lines using the return-to-zero differential phase-shift keying (RZ DPSK) format for information coding

O.V. Shtyrina, A.V. Yakasov, A.I. Latkin, S.K. Turitsyn, M.P. Fedoruk

***Abstract*. The results of mathematical simulation of propagation of optical signals in high-bit-rate dispersion-controlled fibreoptic communication lines are presented. Information was coded by using the return-to-zero differential phase-shift keying (RZ DPSK) format to modulate an optical signal. A number of particular configurations of optical communication lines are optimised in terms of the bit error rate (BER). It is shown that the signal propagation range considerably increases compared to that in the case of a standard return-to-zero on – off keying (RZ OOK) format.**

Keywords: *fibreoptic communication line, information coding, mathematical simulation.*

1. Introduction

The paper is devoted to mathematical simulation of high-bit-rate fibreoptic communication lines (FOCLs) with a distributed dispersion and hybrid (based on amplifiers of different types) amplification schemes using information coding by the phase shift of carrier pulses. In the case of signal modulation in the return-to-zero differential phase-shift keying (RZ DPSK) format, the data are coded by the phase shift between neighbouring pulses. Unlike the standard return-to-zero on – off keying (RZ OOK) format using a pulse to code the logic unit bit and its absence to code the logic zero bit, the logic zero bit in the RZ DPSK format is coded when the phase of an optical pulse in the bit interval is shifted by π with respect to the previous bit, while the logic 1 corresponds to the same phases in two adjacent bits (Fig. 1).

It should be emphasised that we are not dealing here with coherent communication systems because this format does not require the knowledge of the absolute optical phase of a signal. It has been already shown (see, for example, [1 – 4] and references therein) that this format considerably improves the quality of information transfer in optical communication systems compared to the usual digital RZ OOK format.

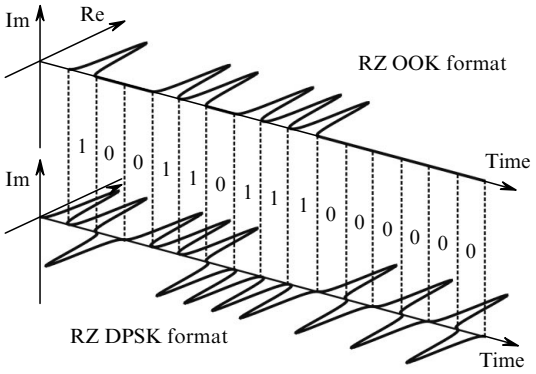

Figure 1. Schematic representation of the RZ OOK and RZ DPSK data formats.

This is caused by three reasons. First, the RZ DPSK format is considerably more stable with respect to the action of parasitic nonlinear effects produced due to cross-phase modulation. In this format, all bit intervals are filled with optical pulses, and the bit-to-bit power distribution is more homogeneous compared to the standard RZ OOK format. Second, it can be expected that the action of four-wave mixing can be reduced due to a random phase shift of the adjacent bits. Third, the method of balanced detection in the RZ DPSK format reduces the bit error rate (BER) compared to the standard RZ OOK format. This allows one to increase the distance between repeaters, the error-free transmission distance, and the capacity of the optical communication system. We formulated mathematically the problem and described particular configurations of fibreoptic communication lines.

2. Mathematical formulation of the problem

It is known that the propagation of an optical signal in a FOCL is described by the generalised nonlinear Schrödinger equation for the complex envelope A of the electromagnetic field amplitude [5]

$$\mathrm{i}\frac{\partial A}{\partial z} + \mathrm{i}\gamma_s(z)A - \frac{\beta_2(z)}{2}\frac{\partial^2 A}{\partial t^2} - \frac{\beta_3(z)}{6}\frac{\partial^3 A}{\partial t^3} +$$

O.V. Shtyrina, M.P. Fedoruk Institute of Computational Technologies, Siberian Branch, Russian Academy of Sciences, prosp. akad. Lavrent'eva 6, 630090 Novosibirsk, Russia; e-mail: shtyrina@ngs.ru, mife@ict.nsc.ru;
A.V. Yakasov Novosibirsk State University, ul. Pirogova 2, 630090 Novosibirsk, Russia e-mail: subj@gorodok.net;
A.I. Latkin Institute of Automation and Electrometry, Siberian Branch, Russian Academy of Sciences, prosp. akad. Koptyuga 1, 630090 Novosibirsk, Russia; e-mail: latkin@gmail.com;
S.K. Turitsyn Aston University, Birmingham, United Kingdom; e-mail: s.k.turitsyn@aston.ac.uk

Received 4 October 2006
Kvantovaya Elektronika **37** (6) 584 – 589 (2007)
Translated by M.N. Sapozhnikov

$$+\sigma(z)\left[|A|^2A+\frac{\mathrm{i}}{\omega_0}\frac{\partial}{\partial t}\left(|A|^2A\right)-T_{\mathrm{R}}A\frac{\partial|A|^2}{\partial t}\right]=0. \quad (1)$$

Here, z is the distance along the line; t is time; $|A|^2$ is the power; β_2 is the group-velocity dispersion parameter; β_3 is the third-order dispersion parameter; T_{R} is the Raman response time; γ_{s} is the effective coefficient taking into account the signal decay and amplification. The quantities β_2, β_3, σ, and γ_{s} are represented as functions of z to take into account their variations in passing from one type of fibre to another. The Kerr nonlinearity coefficient is defined by the expression $\sigma=2\pi n_2/(\lambda_0 A_{\mathrm{eff}})$, where n_2 is the nonlinear refractive index; λ_0 is the carrier wavelength; $\omega_0=c/\lambda_0$ is the radial frequency of the carrier signal; c is the speed of light; A_{eff} is the effective area of an eigenmode of the fibre.

We solved Eqn (1) numerically by the split-step Fourier method (see, for example, [5]).

The operation 'quality' of a communication system is estimated by the BER, which determines the ratio of the number of error bits to the total number of transmitted bits [6]. At present, the admissible value of BER is $\leqslant 10^{-9}$, which corresponds to one erroneously recorded bit per 10^9 communicated bits. Obviously, the direct simulation of such small BER values is virtually impossible and, therefore, various indirect methods are used to estimate the BER in FOCLs.

The bit error rate is estimated, as a rule, by using the concept of the Q factor of a system [6]. In the case of the digital RZ OOK format, assuming that the statistics of zero and unit bits obeys the normal distribution law, we have

$$Q=\frac{\mu_1-\mu_0}{\sigma_1+\sigma_0},$$

where μ_i and σ_i ($i=0, 1$) are the mathematical expectation and root-mean-square deviation for zero and unit bits, respectively.

Then,

$$\mathrm{BER}=\frac{1}{2}\,\mathrm{erfc}\left(\frac{Q}{\sqrt{2}}\right)\approx\frac{\exp(-Q^2/4)}{\sqrt{2\pi}Q}.$$

Note that to the BER $\leqslant 10^{-9}$, the value $Q\geqslant 6$ corresponds.

In this paper, we used the Q factor and the so-called propagation range (defined as the maximum distance for which $Q\geqslant 6$) as criteria for the communication quality. We calculated the propagation range by using pseudorandom sequences with lengths $2^{10}-1\div 2^{14}-1$. The propagation range for a multichannel line was selected as the minimal distance over all frequency channels. In most calculations, we used five frequency channels with the 40-Gbit s^{-1} rate (with the bit interval duration $T_{\mathrm{b}}=25$ ps) in one frequency channel and the adjacent channels separated by the distance $\delta\nu=100$ GHz. Note that separate control calculations were performed in the case of the RZ DPSK format for nine frequency channels, which showed that the propagation range is in fact independent of the number of channels for this data transfer format.

When the RZ DPSK format is used, the calculation of the Q factor should be modified [7, 8]. We compared several alternative approaches. Let us first define the Q factor by the optical phase difference of a signal on a detector. In this case, assuming that the noise statistics is Gaussian, we can define the phase-difference Q factor as [7]

$$Q_{\Delta\Phi}=\frac{\pi}{\sigma_{\Delta\Phi,0}+\sigma_{\Delta\Phi,\pi}},$$

where $\sigma_{\Delta\Phi,0}$ and $\sigma_{\Delta\Phi,\pi}$ are the root-mean-square deviations of the phase difference from 0 and π, respectively. Note that in this case, the value of $Q_{\Delta\Phi}$ is related to the BER by the expression [7]

$$\mathrm{BER}=\mathrm{erfc}\left(\frac{Q_{\Delta\Phi}}{\sqrt{2}}\right).$$

In addition, let us introduce the alternative 'amplitude' Q factor

$$Q_A=\frac{\langle|A_n|\rangle}{\sigma_{|A_n|}}.$$

Here, $|A_n|$ is the optical field amplitude in front of a delay interferometer; n is the bit interval number; and $\sigma_{|A_n|}$ is the root-mean-square deviation of the optical field amplitude. Then, in the case of the RZ DPSK format, the smaller of Q_A and $Q_{\Delta\Phi}$ is used as the Q factor for determining the BER and signal propagation range.

Figure 2 shows the FOCL configurations with the distributed dispersion for which massive numerical calculations were performed. The physical parameters of optical fibres are presented in Table 1.

Before proceeding to the discussion of the results of numerical simulations, we consider mathematical models which are used to describe forward- or backward-pumped

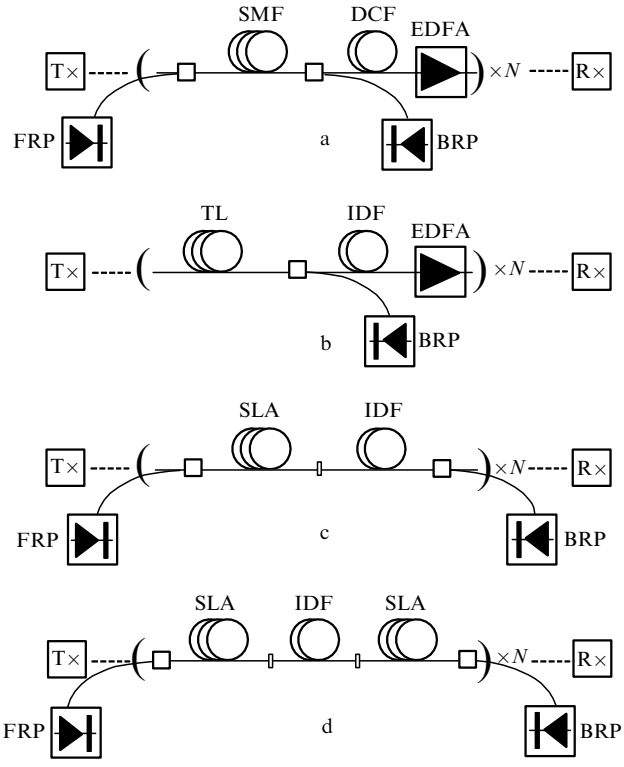

Figure 2. Dispersion FOCL configurations consisting of different combinations of optical fibres SMF, DCF, TL, IDF, and SLA (see Table 1), erbium-doped fibre amplifiers (EDFAs), pump sources for forward (FRP) and backward (BRP) Raman gain, and transmitters (T) and receivers (R). N is the number of FOCL sections.

Table 1. Types of optical fibres and their parameters.

Parameters	Fibres				
	SMF	DCF	SLA	IDF	TL
Losses α_s at the signal wavelength 1550 nm/dB km^{-1}	0.20	0.65	0.188	0.233	0.2
Losses α_p at the pump wavelength 1455 nm/dB km^{-1}	0.25	–	0.234	0.304	0.27
Effective mode area/μm^2	80	19	106	30	65
Dispersion/ps nm^{-1} km^{-1}	17	−100	20.2	−42.3	8.0
Dispersion slope/ps nm^{-2} km^{-1}	0.07	−0.41	0.068	−0.136	0.058
Raman coefficient $\frac{g_R}{A_{eff}}$/W^{-1} km^{-1}	0.42	1.75	0.29	1.2	0.6
Rayleigh scattering coefficient ε_p/km^{-1}	7.05×10^{-5}	9.44×10^{-4}	5.0×10^{-5}	2.2×10^{-4}	1.13×10^{-4}
Rayleigh scattering coefficient ε_s/km^{-1}	5.4×10^{-5}	6.06×10^{-4}	4.0×10^{-5}	1.6×10^{-4}	8.1×10^{-5}
Nonlinear refractive index n_2/m^2 W^{-1}	2.7×10^{-20}	2.7×10^{-20}	2.7×10^{-20}	2.7×10^{-20}	2.7×10^{-20}

lumped erbium-doped fibre amplifiers (EDFAs) and Raman amplifiers.

In the case of EDFAs, the optical signal amplitude was multiplied by $\sqrt{G}$ where G is the signal gain. The spontaneous emission noise was described by a 'white' noise model. The spectral density of the white noise for EDFAs was calculated from the expression

$$S_{sp} = (G-1)n_{sp}h\nu_s, \tag{2}$$

where h is Planck's constant; ν_s is the signal carrier frequency; and n_{sp} is the spontaneous emission coefficient, which is related to the noise factor NF of the amplifier by the expression

$$\mathrm{NF} = \frac{2n_{sp}(G-1)}{G}. \tag{3}$$

Raman amplification was simulated by using a system of ordinary differential equations for the average powers of a signal and pumps taking into account the noises of amplified spontaneous emission (ASE) and double Rayleigh backscattering [9]. In the case of pumping at one wavelength, this model has the form

$$\frac{dP_p^-}{dz} = \alpha_p P_p^- - \varepsilon_p P_p^+ + \frac{\nu_p}{\nu_s}\frac{g_R}{A_{eff}} \times\left\{P_s^+ + P_s^- + 4h\nu_s\Delta\nu_s\left[1+\frac{1}{\exp[h(\nu_p-\nu_s)/kT]-1}\right]\right\}P_p^-,$$

$$\frac{dP_p^+}{dz} = -\alpha_p P_p^+ + \varepsilon_p P_p^- - \frac{\nu_p}{\nu_s}\frac{g_R}{A_{eff}} \times\left\{P_s^+ + P_s^- + 4h\nu_s\Delta\nu_s\left[1+\frac{1}{\exp[h(\nu_p-\nu_s)/kT]-1}\right]\right\}P_p^+,$$

$$\frac{dP_s^+}{dz} = -\alpha_s P_s^+ + \varepsilon_s P_s^- + \frac{g_R}{A_{eff}}(P_p^- + P_p^+) \times\left\{P_s^+ + 2h\nu_s\Delta\nu_s\left[1+\frac{1}{\exp[h(\nu_p-\nu_s)/kT]-1}\right]\right\},$$

$$\frac{dP_s^+}{dz} = \alpha_s P_s^- - \varepsilon_s P_s^+ - \frac{g_R}{A_{eff}}(P_p^- + P_p^+) \times\left\{P_s^- + 2h\nu_s\Delta\nu_s\left[1+\frac{1}{\exp[h(\nu_p-\nu_s)/kT]-1}\right]\right\},$$

where P_s^+, P_s^- and P^+, P^- are the average signal and pump powers propagating forward and backward at the central carrier frequencies ν_s and ν_p, respectively; α_p and α_s are the pump and signal losses, respectively; g_R/A_{eff} is the ratio of the Raman gain to the effective area of the fibre mode; $\Delta\nu_s$ is the total propagation frequency band of the signal (the total frequency band for all frequency channels involved in calculations); and ε_p and ε_s are the coefficients of backward Rayleigh scattering at the pump and signal frequencies, respectively.

The boundary conditions at the beginning ($z = 0$) and the end ($z = L$) of a fibre have the form

$$P_p^-(L) = P_{p0}^-, \quad P_p^+(0) = P_{p0}^+, \tag{4}$$

$$P_s^+(0) = P_{s0}, \quad P_s^-(L) = 0. \tag{5}$$

If signal losses within the fibre were completely compensated by the Raman gain, the boundary condition had the form $P_s^+(L) = P_s^+(0) = P_{s0}$. If different types of fibres were used over the length L, the splice losses were neglected.

By solving the boundary-value problem for the initial system of equations, we calculate the coefficient

$$\alpha_s^{eff}(z) = \alpha_s - \frac{g_R}{A_p}\left[P_p^+(z) + P_p^-(z)\right]$$

and replace $\gamma_s(z)$ by $\alpha_s^{eff}(z)/2$ in Eqn (1).

Let us rewrite the equation for the signal power P_s^+ in the form

$$\frac{dP_s^+}{dz} = -\left\{\alpha_s + \frac{g_R}{A_{eff}}(P_p^- + P_p^+)\right\}P_s^+ + 2h\nu_s\Delta\nu_s\left[1+\frac{1}{\exp[h(\nu_p-\nu_s)/kT]-1}\right]\frac{g_R}{A_{eff}}(P_p^- + P_p^+) + \varepsilon_s P_s^- = -\alpha_s^{eff}(z)P_s^+ + S_1(z) + S_2(z),$$

where

$$S_1(z) = 2h\nu_s\Delta\nu_s\left[1+\frac{1}{\exp[h(\nu_p-\nu_s)/kT]-1}\right] \times\frac{g_R}{A_{eff}}(P_p^- + P_p^+), \quad S_2(z) = \varepsilon_s P_s^-.$$

To take into account the ASE noise, we added random complex quantities η_1 and η_2 to the optical signal amplitude

at each step along z. The correlations of these quantities give $S_1(z)$ and $S_2(z)$, respectively.

3. Results of mathematical simulation

Consider the most important results of calculations on optimisation of FOCLs, presented in Fig. 2. Let us introduce two important parameters $\alpha = G_R/(G_R + G_E)$ and $\eta = G_b/(G_b + G_f)$. Here, G_R and G_E are the gains of the Raman fibre amplifier and EDFA, respectively, and G_b and G_f are the gains of backward- and forward-pumped Raman fibre amplifiers, respectively. Below, we present the results of numerical simulations for different values of parameters α and β. We simulated the propagation of Gaussian pulses with the full width at half-maximum $T_{FWHM} = 12.5$ ps (with the off-duty ratio 50 %).

Consider first the results of mathematical simulation of the FOCL shown in Fig. 2a. The total length of the periodic section of this line was 100 km. Figure 3 presents the counter plots of the propagation range of a signal in the coordinates of average line dispersion $\langle D \rangle$ and average signal power $\langle P \rangle$ for different values of the parameter η. The plot at the right of Fig. 3 shows the dependence of the propagation range on the parameter η for the optimal set of the rest of parameters.

Figure 4 presents the counter plots of the propagation range in the $\langle P \rangle$, $\langle D \rangle$ plane for different values of the parameter α. The plot at the right shows the dependence of the optimal average signal power on the parameter α.

Comparison of the standard binary RZ OOK data transfer format with the RZ DPSK format is shown in Fig. 5 demonstrating the counter plots of the propagation range in the $\langle D \rangle$, $\langle P \rangle$ plane and the dependences of the

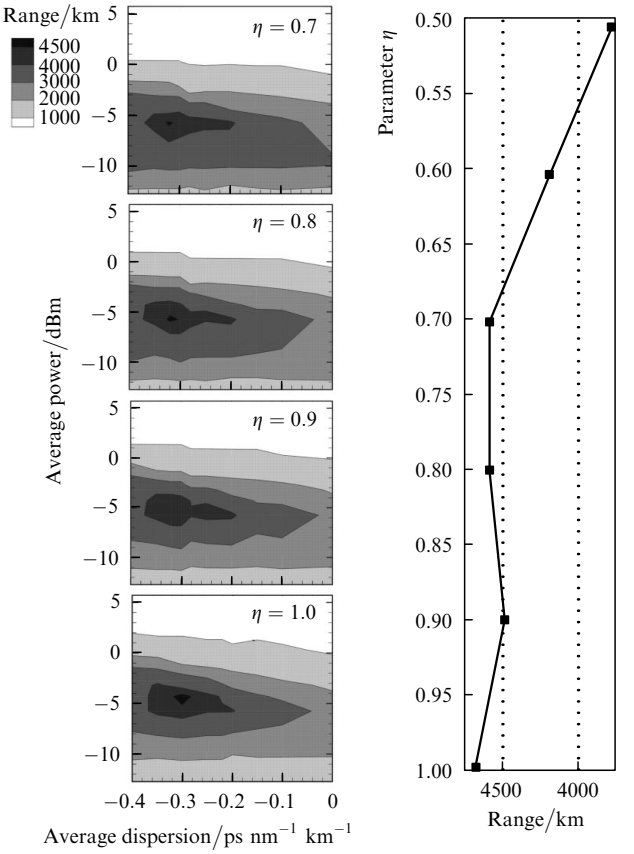

Figure 3. Counter plots of the signal propagation range in the $\langle D \rangle$, $\langle P \rangle$ plane for different configurations η (the FOCL configuration in Fig. 2a).

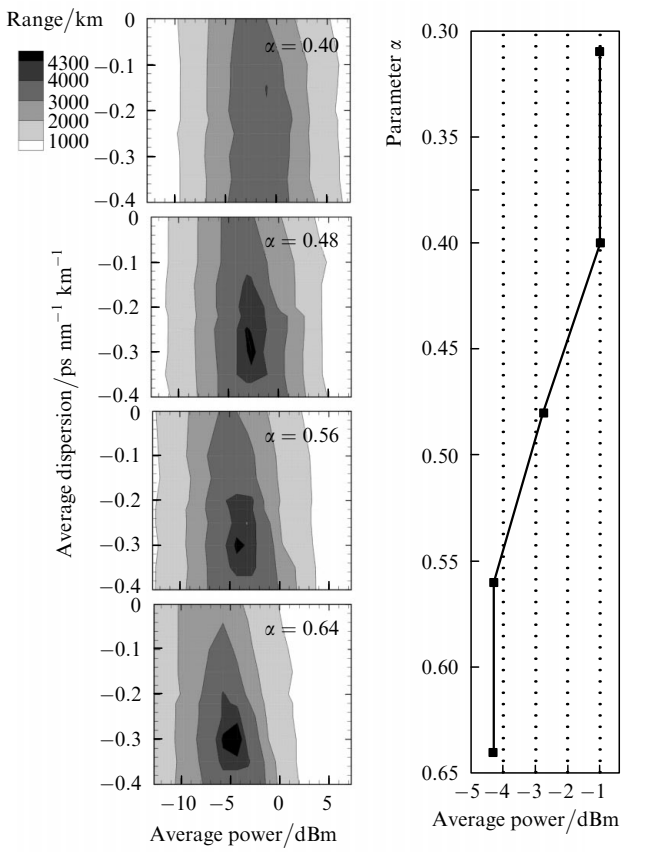

Figure 4. Counter plots of the propagation range in the $\langle P \rangle$, $\langle D \rangle$ plane for different α (the FOCL configuration in Fig. 2a).

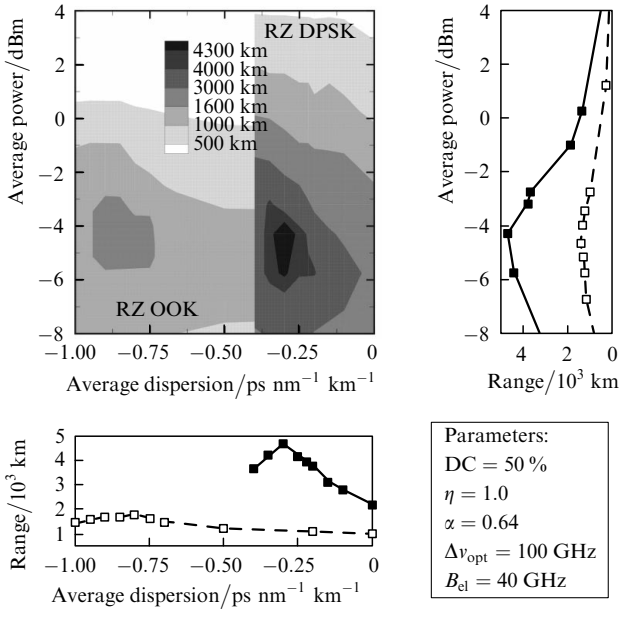

Figure 5. Counter plots of the signal propagation range in the $\langle D \rangle$, $\langle P \rangle$ plane for the RZ OOK (□) and RZ DPSK format (■) for the pulse off-duty ratio 50 %, $\eta = 1.0$, $\alpha = 0.64$, the frequency cannel separation 100 GHz and the band of width 40 GHz.

propagation range on the average signal dispersion and average signal power for the optimal set of the rest of parameters. One can see that the RZ DPSK format considerably improves the performance of the system compared to the standard RZ OOK format.

Let us now present the results of optimisation of the FOCL with a periodic section shown in Fig. 2b. Figure 6 shows the counter plots of the propagation range in the $\langle P\rangle$, $\langle D\rangle$ plane for different values of the parameter α. One can see that, irrespective of α, the maximum of the propagation range is observed for the average pulse power $\langle P\rangle \simeq -0.3 \div 0$ dBm and the average dispersion $\langle D\rangle \simeq -0.1 \div 0.2$ ps nm^{-1} km^{-1}. However, as the propagation range increases up to $\sim 4000 - 4500$ km, the region of admissible parameters $\langle D\rangle$ and $\langle P\rangle$ drastically narrows down. Figure 6 shows (at the right) the dependence of the average signal power, for which the optimal propagation range is achieved, on the parameter α for the optimal values of $\langle D\rangle$. The optimal average signal power decreases monotonically with increasing α.

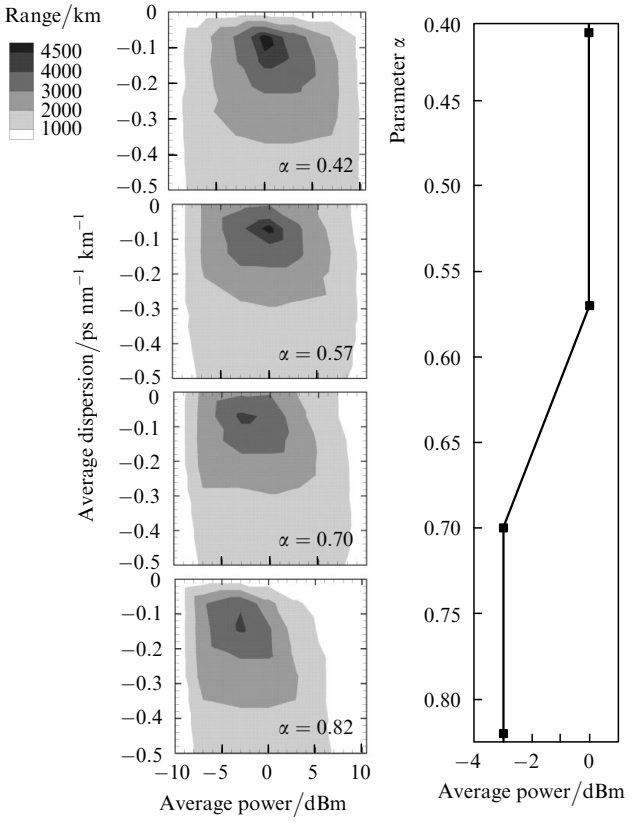

Figure 6. Counter plots of the signal propagation range in the $\langle P\rangle$, $\langle D\rangle$ plane for different α (the FOCL configuration in Fig. 2b).

This behaviour can be qualitatively explained as follows. Consider first the case of $\alpha = 0$. The main factors determining the propagation of a pulse (by neglecting noise) are the Kerr nonlinearity, whose contribution is proportional to the pulse power averaged over the section (along z), and the average dispersion $\langle D\rangle$ of the line. In this case, as was shown, the maximum propagation range is achieved when the average dispersion has a negative value compensating the Kerr nonlinearity, i.e. when the balance between the average power and the dispersion of the line is observed. It is obvious that the section-averaged signal power is proportional to the input average power $\langle P\rangle$. Amplification due to backward Raman pumping inside the section results in the increase in the section-averaged signal power for the same input average power $\langle P\rangle$. This means that to maintain balance between nonlinearity and dispersion, it is necessary to reduce the value of $\langle P\rangle$ at the section input, which is observed in Fig. 6.

Finally, we consider the results of numerical simulation of the lines shown in Figs 2c, d and study the influence of the preliminary cumulative dispersion D_{pre} on the transfer characteristics of these systems. In the case of asymmetric dispersion configuration (Fig. 2c), the propagation range is maximal for $\eta = 0.5$. The maximal propagation range equal to 5750 km is achieved for the average signal power of -9.75 dBm, the average dispersion of the line $\langle D\rangle = -0.2$ ps nm^{-1}km^{-1} and the initial cumulative dispersion $D_{\text{pre}=} -75$ ps nm^{-1}km^{-1} (Fig. 7a). If the coefficient η is increased, the maximal propagation range is achieved for a higher average signal power. For example, for $\eta = 0.7$, we have $\langle P\rangle = -5.75$ dBm.

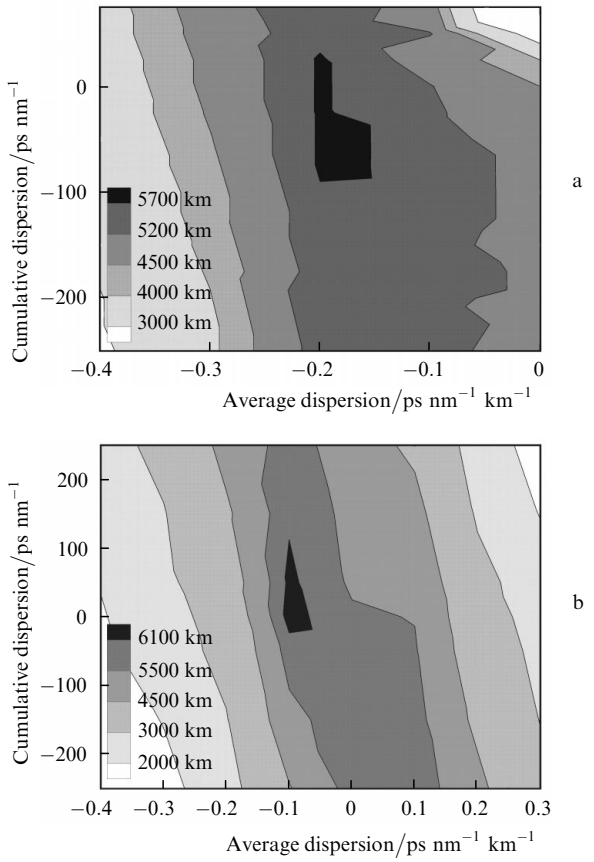

Figure 7. Counter plots of the signal propagation range in the $\langle D\rangle$, D_{pre} plane for $\eta = 0.5$ (the FOCL configuration in Fig. 2c) (a) and 0.9 (the FOCL configuration in Fig. 2d) (b).

Figure 7b shows the counter plots of the propagation range in the $\langle D\rangle$, D_{pre} plane for the symmetric dispersion configuration (Fig. 2d). In this case, the maximal propagation range equal to 6300 km is achieved for $\eta = 0.9$, $D_{\text{pre}} = 0$, $\langle D\rangle = -0.1$ ps nm^{-1} km^{-1} and the output average power $\langle P\rangle = -5.75$ dBm. A considerable increase in the maximal propagation range for this dispersion configuration

is explained by the fact that the IDF is optimally located with respect to Raman pump sources. Indeed, such a location of the fibre reduces the influence of multiple-beam interference due to double Rayleigh backscattering. Note that multiple-beam interference plays a significant role when pumping is performed directly into the IDF, as in the case of the dispersion configuration shown in Fig. 2c.

4. Conclusions

We have simulated high-bit-rate FOCLs with the dispersion control based on information coding by using the RZ DPSK format. Particular FOCL configurations with different variants of the optical gain have been optimised and the region of optimal parameters for these systems has been determined. The transfer characteristics in a standard single-mode fibre have been compared for the RZ OOK and RZ DPSK formats and it has been shown that the propagation range in the latter case is considerably greater.

Acknowledgements. This study was supported by the Integration Interdisciplinary Project of the Siberian Branch, RAS (Grant No. 31), the Ministry of Education and Science of the Russian Federation (Grant No. 13-06-01) and INTAS (Grant No. 03-56-203).

References

1. Gnauck A.H. et al. *Proc. OFC 2002* (Anaheim, CA, 2002) Postdeadline Paper FC2.
2. Zhu B. et al. *ECOC 2002* (Copenhagen, Denmark, 2002) Postdeadline paper PD4.2.
3. Bissessur H., Charlet G., Gohin E., Simonneau C., Pierre L., Idler W. *Proc. ECOC 2002* (Copenhagen, Denmark, 2002) paper 8.1.2.
4. Liu X., Wei X., Slusher R.E., McKinstrie C.J. *Opt. Lett.*, **27**, 1616 (2002).
5. Agrawal G.P. *Nonlinear Fiber Optics* (New York: Academic Press, 2001).
6. Agrawal G.P. *Fiber-Optic Communication systems* (New York: John Wiley & Sons, INC, 1997).
7. Wei X., Liu X., Xu C. *IEEE Photonic. Technol. Lett.*, **15** (11), 1636 (2003).
8. Xu C., Liu X., Wei X. *IEEE J. Sel. Top. Quantum Electron.*, **10** (2), 281 (2004).
9. Kidorf H. et al. *IEEE Photonic. Technol. Lett.*, **11**, 530 (1999).